

LA-UR-15-27014

Approved for public release; distribution is unlimited.

Title: Evaluation of Pulsed Sphere Time-of-Flight and Neutron Attenuation Experimental Benchmarks Using MCNP6's Unstructured Mesh Capability

Author(s): Joel A. Kulesza
Roger L. Martz

Intended For: Nuclear Technology

Issued: September 2015



Disclaimer: Los Alamos National Laboratory, an affirmative action/equal opportunity employer, is operated by the Los Alamos National Security, LLC for the National Nuclear Security Administration of the U.S. Department of Energy under contract DE-AC52-06NA25396. By approving this article, the publisher recognizes that the U.S. Government retains nonexclusive, royalty-free license to publish or reproduce the published form of this contribution, or to allow others to do so, for U.S. Government purposes. Los Alamos National Laboratory requests that the publisher identify this article as work performed under the auspices of the U.S. Department of Energy. Los Alamos National Laboratory strongly supports academic freedom and a researcher's right to publish; as an institution, however, the Laboratory does not endorse the viewpoint of a publication or guarantee its technical correctness.

Abstract

This report extends the verification and validation of MCNP6's unstructured mesh (UM) features for neutron transport capabilities by comparing code and experimental results for two different sets of experiments. The first set of experiments analyzed are time-of-flight spectrum measurements of spheres pulsed by 14 MeV neutrons performed by Lawrence Livermore National Laboratory in the early 1970s. The second set of experiments are spontaneous fission neutron attenuation measurements in relatively simple geometries with varying shield thicknesses performed by Ueki et. al in the early 1990s. First, traditional constructive solid geometry (CSG) models are analyzed to ensure agreement with experimental values and to form a basis of comparison with UM results. For the pulsed sphere experiments, a series of UM calculations are performed using first-order tetrahedral elements with various levels of mesh refinement. For the Ueki experiments, purely CSG, purely UM, and hybrid CSG/UM calculations are performed using first- and second-order tetra- and hexahedral elements. In the purely UM cases, two different meshing algorithms are used to specify the first-order tetrahedral mesh. The pulsed sphere calculated and experimental time-of-flight spectra agree with p -values greater than 0.999 when compared using χ^2 goodness-of-fit tests. Furthermore, UM results show discrepancies with the experimental values comparable to CSG cases. The Ueki neutron attenuation calculated values using track length and point detector tallies agree with the experimental values within 1σ with a single exception that agrees well within 2σ . As such, we conclude that the results for CSG and UM calculations agree amongst themselves and with the experimental quantities when considering the associated statistical uncertainties.

Keywords

Experimental Benchmark Comparison, MCNP, Unstructured Mesh

I. Introduction

This paper reports results for calculations performed using MCNP6's unstructured mesh (UM) capabilities based on two sets of experimental benchmarks. This work is used to broaden the verification and validation (V&V) suite of problems for MCNP6's UM capabilities and, along the way, helped to improve the robustness of the UM tracking algorithms by showing weaknesses in the point detector routines that have subsequently been rectified. A subset of the cases herein are expected to be included in a future MCNP6 V&V suite release.

The first set of experiments were performed at Lawrence Livermore National Laboratory (LLNL) in the early 1970s and consist of time-of-flight spectrum measurements resulting from spheres of various materials pulsed with 14 MeV neutrons (Ref. 1). These experiments are chosen because they provide validation of time-dependent quantities (something not yet extensively tested with MCNP6's UM capabilities). Also, these experiments use geometries that are traditionally difficult to model with unstructured mesh (i.e., curved surfaces and/or thin spherical shells). These features allow us to examine the sensitivity of the results to various levels of mesh refinement relative to the traditional constructive solid geometry (CSG) results in the current shielding validation suite.

The second set of experiments discussed herein are spontaneous fission neutron attenuation sensitivity measurements performed by Ueki et. al. in the early 1990s (Ref. 2). Note that this set of experiments is subtly different from the benchmark experiments described in Reference 3 (noted to avoid confusion because of the similarity and the greater availability of Reference 3). Regardless, the experimental benchmark used herein is chosen because it is characterized by simple but non-trivial geometry and continues to be used to validate both transport methods (Ref. 4) and nuclear data (Ref. 5), and is thus well-studied and understood.

Both sets of experiments are analyzed using CSG and UM geometry. For the pulsed spheres, the UM consists of strictly first-order tetrahedral elements with various levels of mesh refinement. However, for the Ueki benchmark the UM consists of first- and second-order (linear and quadratic) tetra- and hexahedral elements and a single level of refinement for each element type. As such, this report provides a set of results for two experimental benchmarks that can be used to validate time-dependent and time-independent neutron behavior for a variety of UM element types.

II. LLNL Pulsed Sphere Descriptions

The LLNL pulsed sphere experiments studied a series of materials in various configurations. Sometimes identical materials in different geometric configurations were used to investigate pulse spectrum behavior resulting from attenuation through various thickness of the material. Of the experiments conducted, six unique material and geometric configurations are selected for analysis herein. The experiments analyzed will be described specifically in the following subsections with the MCNP6 validation suite identifiers in parentheses should the reader wish to locate the CSG models within his or her existing `MCNP6/Testing/VALIDATION_SHIELDING` directory.

II.A. Experimental Setup Overview

All spheres feature a channel through half of the sphere that permits insertion of the target assembly used to produce the 14 MeV source neutrons. Assuming that the target assembly enters the sphere through the channel from the $+x$ direction, the detector package is positioned relative to the $-x$ direction. Note that the detector package is modeled as a ring detector within MCNP6 because of geometric and source symmetry. For each experiment, the detector is either a Pilot-B or NE213 scintillator and associated hardware, with the response functions given in Reference 6. When describing the spherical geometry, the dimensions are given in terms of 14 MeV neutron mean free paths (m.f.p.) along the flight path from the source to the detector and also the outer radius of the sphere in centimeters.

II.B. Beryllium Sphere (BE08 / lps_berl)

The beryllium sphere with a thickness of 0.8 m.f.p. (outer radius of 12.58 cm) consists of a spherical shell with a cylindrical channel and spherical hollow core as shown in Figure 1a. A Pilot-B detector with a 1.6 MeV cutoff energy and FWHM resolution of 4 ns is positioned 30° off-axis with a flight path distance of 765.2 cm. The detector captured results from 137 to 409 ns (corresponding to neutron energies of 1.8 to 16.7 MeV).

II.C. Carbon Sphere (C29 / lps_carbon)

The carbon sphere with a thickness of 2.9 m.f.p. (outer radius of 20.96 cm) consists of a spherical shell with a cylindrical and tapered round channel leading to the center as shown in Figure 1b. A NE213 detector with a 1.6 MeV cutoff energy and FWHM resolution of 4 ns is positioned 30° off-axis with a flight path distance of 766.0 cm. The detector captured results from 141 to 409 ns (corresponding to neutron energies of 1.8 to 15.8 MeV).

II.D. Concrete Sphere (CCR20 / lps_conc)

The concrete sphere with a thickness of 2.0 m.f.p. (outer radius of 21 cm) consists of a spherical shell with a tapered round channel leading to a hollow spherical center cavity as shown in Figure 1c. A NE213 detector with a 1.6 MeV cutoff energy and FWHM resolution of 3 ns is positioned 120° off-axis with a flight path distance of 975.4 cm. The detector captured results from 185 to 491 ns (corresponding to neutron energies of 2.1 to 14.9 MeV).

II.E. Iron Sphere (FE09 / lps_iron)

The iron sphere with a thickness of 0.9 m.f.p. (outer radius of 4.46 cm) consists of a spherical shell with a tapered round channel leading to the center as shown in Figure 1d. A NE213 detector with a 1.6 MeV cutoff energy and FWHM resolution of 3 ns is positioned 30° off-axis with a flight path distance of 766.0 cm. The detector captured results from 137 to 417 ns (corresponding to neutron energies of 1.8 to 16.8 MeV).

II.F. Water Sphere (H2O19 / lps_water)

The water sphere with a thickness of 1.9 m.f.p. (outer radius of 22.55 cm) consists of a spherical steel shell (0.15 cm) filled with water surrounded by another steel shell (0.06 cm) with a vacuum between both shells. Each shell has a tapered round channel leading to the center as shown in Figure 1e. A Pilot-B detector with a 1.6 MeV cutoff energy and FWHM resolution of 5 ns is positioned 30° off-axis with a flight path distance of 754.0 cm. The detector captured results from 126 to 392 ns (corresponding to neutron energies of 1.9 to 19.3 MeV).

II.G. Lithium Sphere (LI616 / `lps_lith`)

The Lithium-6 sphere with a thickness of 1.6 m.f.p. (outer radius of 25.52 cm) consists of three steel shells (each 0.058 cm thick) with lithium filling the region between each shell. The inner shell has a tapered round channel leading to the center with the two outer shells having a cylindrical channel as shown in Figure 1f. A Pilot-B detector with a 1.6 MeV cutoff energy and FWHM resolution of 4 ns is positioned 30° off-axis with a flight path distance of 765.2 cm. The detector captured results from 133 to 409 ns (corresponding to neutron energies of 1.8 to 17.8 MeV).

II.H. CSG and UM Model Overview

The aforementioned six pulsed sphere experiments were also analyzed previously using two different levels of geometric, material, source, and tally specificity as part of the MCNP6 shielding validation suite (Ref. 7). The models with less specificity (i.e., “Legacy”) models contain only the geometry of the spheres themselves whereas the “Detailed” models contain the sphere, the target assembly that emits the 14 MeV neutrons, and some external geometry such as beam lines. The Detailed models also contain detailed source and tally specifications relative to the Legacy models and somewhat different material compositions.

For the UM models analyzed herein, only the spherical geometry is modeled so the Legacy models form the fairest basis for comparison. However, UM results are compared to both the CSG Legacy models (which had time-of-flight tallies added), the CSG Detailed models (which have pre-existing explicit time-of-flight tallies), and newly-constructed CSG Hybrid models that contain only the simplistic geometry but the source, material, and tally definitions from the Detailed models. All UM solid models are constructed using SpaceClaim Engineer 2014 (Ref. 8) which are then meshed and used to generate MCNP6 input files with Attila4MC (Ref. 9). When generating the UM, Attila4MC’s Curvature Refinement (advanced) option is used extensively to specify maximum d/h (i.e., the distance d of the model edge curve from the mesh edge divided by the mesh size h) and minimum mesh edge length. For each experiment, a variety of refinement levels are used to determine the sensitivity of results to the mesh size. The refinement levels, generating parameters, and resulting mesh descriptions are summarized in Table I. Like the pre-existing validation suite cases, no variance reduction is introduced beyond the default techniques enabled (i.e., weight cutoff and

implicit capture for the random transport and the default point detector roulette game) for both CSG and UM calculations. Materials and sources in the UM cases are defined consistent with the Legacy CSG models.

Note that for processing the MCNP6 calculated results, a multi-step process is used to properly normalize the time spectra. Following a procedure described by work performed in 2011 (Ref. 10), time-of-flight spectra are renormalized with the `fm` card using the following procedure that necessitates three sequential calculations:

1. Set all cell materials and densities corresponding to air. Calculate the normed average tally per history, \bar{x}_{Air} , reported by MCNP6 for the time-of-flight spectrum tally,
2. Run the nominal material calculation with an `fm` card equivalent to $1/\bar{x}_{\text{Air}}$ and integrate the resulting discrete time-of-flight spectrum, which is denoted $S_{\text{Calc.}}$, and finally
3. Run the nominal material calculation with an `fm` card equivalent to

$$\frac{1}{\bar{x}_{\text{Air}}} \frac{S_{\text{Exp.}}}{S_{\text{Calc.}}}$$

where $S_{\text{Exp.}}$ is the integral of the discrete experimental spectrum.

For the purposes herein, all normalization values are considered to be “best estimate” so no error propagation to the final results is performed. When performing normalizations and comparisons, it is important to recognize that the benchmark times are given in nanoseconds whereas MCNP6 specifies times in “shakes” where 1 shake is equivalent to 10 nanoseconds. Nevertheless, in all cases the calculated tally time bin structure is consistent with the corresponding experimental time bin structure.

III. Ueki Benchmark Description

The Ueki benchmark suite is a series of experiments characterized by a small spontaneous fission Cf-252 source centered within a paraffin cube with a conical cutout facing a detector, with one or several shields of thickness T between the source and detector as shown in Figure 2. Of the configurations provided in the experimental description (Ref. 2), this analysis focuses on those configurations with a single graphite shield of

either thickness $T = 2, 5, 10, 15, 20, 25, 30$, or 35 cm. This benchmark was most-recently analyzed in Ref. 4 where it is noted that tabulated results are not provided for the cases with the graphite shield. As such, the lin-log plot provided in Ref. 4's Fig. 7-2 is digitized to extract the experimental dose attenuation factors for graphite. When this digitization is performed, a conservative 5% uncertainty is assigned to account for experimental and digitization errors.

The experiments are modeled using both CSG and UM with both a small cubic F4 (track-length) tally with an F5 (point detector) tally centered within the cube; Ref. 4 did likewise but for CSG only. Unlike Ref. 4, no variance reduction is performed beyond the default techniques enabled (i.e., weight cutoff and implicit capture for the random transport and the default point detector roulette game). This approach is taken in order to understand the unperturbed rate of problem convergence for both geometries. Both CSG and UM models use materials for paraffin, graphite, and air based on the compositions and densities provided in Reference 11. For both geometries, the source is positioned at $x = 0.001$ cm in order to prevent it from being coincident with CSG cell or UM pseudocell boundaries. The source is specified with an energy distribution following the MCNP6 Watt fission spectrum (function -3) using MCNP6 distribution parameters $a = 1.025$ and $b = 2.926$. When specifying the two tallies, the dose response function from Reference 12 is used and the results are normalized to $\text{Sv}\cdot\text{hr}^{-1}\cdot\text{source-particle}^{-1}$. Because the benchmark results are given as dose attenuation factors, once the calculations are performed the calculated shielded results are normalized to the unshielded value. Finally, the calculated values are normalized relative to the experimental values for easier interpretation.

Two methods for generating the UM input file are used here. At present MCNP6 only supports UM specified using an Abaqus mesh input file format (Ref. 13). As such, the analyst can use Abaqus to create the mesh input file after creating (or importing) the geometry, assigning materials and element sets, and creating the mesh. More details regarding working with MCNP6's UM capabilities in this regard are given in Reference 14 with a direct illustration using Abaqus (to create geometry similar to the Ueki experiment with a 20 cm graphite shield) given in Reference 15. Once the Abaqus mesh input file is created, the `um_pre_op` utility provided with MCNP6 can be used to generate a skeleton MCNP6 input file. Alternatively, one can use Attila4MC to prepare Abaqus-formatted UM and MCNP6 input files as done with the pulsed sphere

experiments. Note that Abaqus is capable of generating mesh using first- and second-order tetra-, penta-, and hexahedral elements whereas Attila4MC is only capable of generating mesh using first-order tetrahedrons.

Abaqus is used to generate unstructured mesh using first- and second-order tetra- and hexahedral elements to compare the effect (which should be minimal) of using different element types. Furthermore, hybrid geometry cases are created with either the paraffin or shield/detector defined as CSG and the remainder as UM to validate cases where it is appropriate to combine CSG and UM. Regardless, when generating a mesh with Abaqus, a ‘seed’ is needed to roughly define edge length. When tetra- and hexahedral mesh (both first- and second-order) are seeded, the same seed value is used so the resulting mesh is on as consistent a basis as possible. Some minor differences are expected in the results because the conical cutout in the paraffin cannot be represented exactly using UM and particle positions on the surfaces will be different and subsequently affect the particle tracking.

In addition, Attila4MC is used to generate unstructured mesh using first-order tetrahedral elements in order to see the effect of a different meshing algorithm on the results. Like the pulsed sphere experiments, when using Attila4MC Curvature Refinement is applied with a maximum $d/h = 0.02$ and a minimum edge length of 1 cm. The Attila4MC-generated models are entirely of the UM variety since Attila4MC does not handle CSG; ample validation of hybrid geometries is provided with the Abaqus model calculations.

IV. Calculation Results

Each of the calculations use a consistent “bleeding edge” (i.e., nightly-build) version of MCNP6, version 6.1.2. The latest nuclear data libraries supplied with MCNP6 are used. The pulsed sphere calculations use libraries consistent with the validation suite cases (ACTIA and ENDF66A based on ENDF/B-VI.8 and -VI.0, respectively). The Ueki calculations use the default library for each material’s constituent isotope (ENDF71X, ENDF7SAB, and RMCCSA based on ENDF/B-VII.1, ENDF/B-VII.0, and LLNL evaluations, respectively). All calculations are performed on the Los Alamos National Laboratory Mapache supercomputer. Mapache consists of 592 compute nodes hosting dual-socket quad-core Intel Nahalem processors (4,736 processing cores total) interconnected with InfiniBand with calculations distributed through the Moab Workload Manager. Each pulsed sphere CSG and UM calculation used 8 processors and each Ueki calculation used between 16

and 64 processors in order to balance queue throughput and speed of execution while keeping all calculations well below an administratively-imposed wall time limit. The pulsed sphere Legacy CSG models use 1M histories with Hybrid and Detailed CSG models use 10M (all consistent with the MCNP6 validation suite). All pulsed sphere and Ueki UM models use 1M histories.

IV.A. Pulsed Sphere Results

The pulsed sphere calculated spectra are shown in Figure 3 for the six experiments studied. Note that the line plots are colored based on the ColorBrewer2 8-class Paired color set (Ref. 16) in the electronic version of this paper. Additional effort is not made to differentiate the datasets (in the print or electronic versions of this paper) on a given plot because of the generally high level of agreement for the purposes of our comparisons herein.

For all calculations, the agreement between the experimental and calculated spectra is qualitatively confirmed through visual inspection. One abnormality is apparent in Figure 3c around 310 ns — a step change in the calculated response relative to the benchmark. This artifact is not visible in recent published work (Fig. 48 of Ref. 17) and it would be interesting to identify the reason for this. Regardless, using a χ^2 goodness-of-fit test shows that unnormalized and normalized calculated and experimental spectra agree with p -values greater than 0.999 in all cases which supports a null hypothesis that a given calculated spectrum behaves comparably to the experimental spectrum.

Next, the fractional errors, ϵ , between the calculated and experimental spectra are determined with

$$\epsilon = \frac{\int_0^\infty [f_{\text{Exp.}}(t) - f_{\text{Calc.}}(t)]^2 dt}{\int_0^\infty [f_{\text{Exp.}}(t)]^2 dt} \rightarrow \frac{\sum_t (f_{t,\text{Exp.}} - f_{t,\text{Calc.}})^2}{\sum_t (f_{t,\text{Exp.}})^2} \quad (1)$$

by recognizing that all time bin widths are identical and that there are an equal amount of bins in the calculated and experimental results. These fractional errors are shown in Table II and it should be recognized that unlike previous work in Reference 10, no points are excluded from either the χ^2 p -value or fractional error calculations. Furthermore, the error observed in the UM models agrees most closely with the Legacy models while the Detailed and Hybrid models behave similarly. Because the geometry in the Legacy and Hybrid models is identical, differences between the UM calculations and the more detailed CSG and experimental

results can be attributed to material, source, and external geometry differences rather than the spherical geometry. Regardless, we can conclude that the pulsed sphere UM models adequately agree with the CSG and experimental results. This statement is true for all levels of mesh refinement, suggesting a relatively low sensitivity to mesh refinement as long as the mesh is a reasonable representation of the intended configuration and does not feature any defects or artifacts. For this work, the UM was generated finely enough to keep the mass of the spheres consistent with the CSG geometry within 1% for the spheres, within 2% for the water sphere’s shell, and within 3% for the lithium sphere’s shell.

IV.B. Ueki Neutron Attenuation Results

As noted previously, the Ueki calculations can be roughly divided into three groups: those with strictly UM, those with the paraffin as UM and the shield/detector as CSG, and those with the paraffin as CSG and the shield/detector as UM. The results for the strictly UM (and strictly CSG) calculations are shown in Figure 4. The results for the hybrid cases with the paraffin as UM are shown in Figure 5 and the results for the hybrid cases with the paraffin as CSG are shown in Figure 6.

In Figure 4, both the F4 and F5 tallies show agreement with the experimental attenuation values within 1σ with the sole exception of the Attila4MC F4 tally corresponding to a 25 cm thick graphite shield (which narrowly misses the 1σ criterion but agrees well within 2σ). For the hybrid case results shown in Figures 5 and 6, the F4 and F5 tallies show agreement with the experimental attenuation values within 1σ without exception. Observe that the results shown in Figure 6 are identical because the UM represents purely Cartesian components and because of the identical seeding the mesh elements have the same boundaries. As such, particles that make it to either tally will undergo identical surface crossings and thus register the same score.

In addition, perspective half-space qualitative F4 flux edits are provided in Figure 7 for the purely UM cases with first-order elements to (a) provide an overall view of the flux behavior to validate its appropriateness and (b) illustrate one of the benefits of using UM: minimal-overhead geometry-specific unstructured mesh-based results visualization. Only linear elements are shown for demonstration purposes, but other UM results appear similarly. Looking at the mesh and edits, a couple observations can be made:

1. The Abaqus-generated mesh features the graphite shield divided into a series of shields (parts) in order to re-use identical mesh input files in a number of cases. Each of the parts is assigned a different material (graphite or air) within MCNP6 to represent the various shield thicknesses. While this leads to an unnecessarily refined mesh within the shield it reduces the file handling (and subsequent quality control) burden.
2. The Curvature Refinement feature within Attila4MC has a clear local effect on the mesh when comparing the mesh size around the conical cutout in the paraffin versus those in the shield. This feature provides a convenient way to allow precise geometric representation without unduly fine mesh throughout the model.
3. Because of how the F4 flux edits are calculated, a coarse mesh (such as the one shown in Attila4MC shield) will yield less information than a fine mesh (such as in the Abaqus cases). The coarse mesh is adequate to represent the geometry; however, it is less useful when visualizing the resulting particle distribution.

As such, the user is cautioned to specify the UM resolution considering both appropriate representation of the geometry versus mesh size (and thus element count) as well as the intended use of the UM edits from a post-processing and visualization standpoint.

V. Conclusions

The pulsed sphere calculated and experimental time-of-flight spectra agree with a p -value greater than 0.999 when compared with χ^2 goodness-of-fit tests with the UM cases showing discrepancies from the experiment comparable to the discrepancies shown by the CSG cases. The Ueki neutron attenuation calculated values using F4 and F5 tallies agree with the experimental values within 1σ except for a single point that agrees well within 2σ . Qualitatively, we can see that the behavior of all calculated results in terms of magnitude and trends are reasonable. As such, we conclude that the results for CSG and UM calculations agree amongst themselves and with the experimental quantities when considering the associated statistical uncertainties. This conclusion and work thus extends the V&V basis for MCNP6's UM capabilities.

Future work includes performing equivalent analyses with first- and second-order pentahedral elements. This is not done in the present work because these elements tend to be used much less frequently than tetra- and hexahedral elements and the tracking routines for them are a combination of the tetra- and hexahedral routines. It would also be interesting to investigate the cause for the step in the concrete sphere time-of-flight spectrum at approximately 310 ns. While it is likely not the result of a nuclear data issue, it would also be interesting to investigate the effect of using the most current nuclear data on the time-of-flight spectra for all spheres investigated herein similar to what was done in Ref. 17. Finally, no variance reduction is performed for the analyses herein. While it is unnecessary for the pulsed spheres, it would be compelling to investigate the behavior and figure-of-merit of the tallies when different variance reduction techniques are applied to the Ueki benchmark. These techniques might include (pseudo)cell-based importances or weight windows and mesh-based weight windows generated with the MCNP6 weight window generator or an external utility such as Attila4MC and/or ADVANTG. Note that one advantage (no pun intended) to mesh-based weight windows is that they transcend the geometry type used so a single set of weight windows can be applied to CSG, UM, or hybrid geometry calculations.

Acknowledgements

The authors wish to thank Joel M. Risner of Oak Ridge National Laboratory for providing electronic reference cases for the Ueki experiments in order to validate pre-existing input parameters and to confirm the experimental configuration. The authors also thank Gregory A. Failla and Ian M. Davis of Varian Medical Systems for providing licenses and expert insights to permit the use of SpaceClaim and Attila4MC for this work.

VI. References

- [1] C. Wong *et. al.*, “Livermore Pulsed Sphere Program: Program Summary Through July 1971,” Tech. Rep. UCRL-51144, Rev. 1, Lawrence Livermore National Laboratory, Livermore, CA, USA, 1972.
- [2] K. Ueki, A. Ohashi, and Y. Anayama, “Neutron Shielding Ability of KRAFTON N2 — Mannan — KRAFTON N2 Sandwich-type Materials and Others.,” in *Radiation Protection and Shielding Division Topical Meeting*, (Pasco, WA, USA), American Nuclear Society, April 26 – May 1, 1992.
- [3] K. Ueki *et. al.*, “Systematic Evaluation of Neutron Shielding Effects for Materials,” *Nuclear Science and Engineering*, vol. 124, pp. 455–464, 1996.
- [4] S. W. Mosher *et. al.*, “ADVANTG — An Automated Variance Reduction Parameter Generator,” Tech. Rep. ORNL/TM-2013/416, Oak Ridge National Laboratory, Oak Ridge, TN, USA, 2013.
- [5] J. M. Risner *et. al.*, “Production and Testing of the VITAMIN-B7 Fine-Group and BUGLE-B7 Broad-Group Coupled Neutron/Gamma Cross-Section Libraries Derived from ENDF/B-VII.0 Nuclear Data,” Tech. Rep. NUREG/CR-7045 (ORNL/TM-2011/12), Oak Ridge National Laboratory, Oak Ridge, TN, USA, 2011.
- [6] E. F. Plechaty and R. J. Howerton, “Calculational Models For LLL Pulsed Spheres (CSEWG Shielding Benchmark Collection No. SDT 10),” Tech. Rep. UCID-16372, Lawrence Livermore National Laboratory, Livermore, CA, USA, 1973.
- [7] J. T. Goorley *et. al.*, “Initial MCNP6 Release Overview — MCNP6 version 1.0,” Tech. Rep. LA-UR-13-22934, Los Alamos National Laboratory, Los Alamos, NM, USA, 2013.
- [8] SpaceClaim Corporation, “SpaceClaim Engineer 2014.” <http://http://www.spaceclaim.com/en/default.aspx>, 2014. Accessed: 2015-08-10.
- [9] Varian Medical Systems, “Attila with MCNP Integration: Attila4MC.” <http://www.transpireinc.com/html/attila>, 2015. Accessed: 2015-08-25.
- [10] A. S. Bennett and B. C. Kiedrowski, “Revisiting the MCNP Shielding Validation Suite,” Tech. Rep. LA-UR-11-04540, Los Alamos National Laboratory, Los Alamos, NM, USA, 2011.

- [11] R. J. McConn Jr. *et al.*, “Compendium of Material Composition Data for Radiation Transport Modeling,” Tech. Rep. PNNL-15870, Rev. 1, Pacific Northwest National Laboratory, 2011.
- [12] “Neutron and Gamma-Ray Flux-to-Dose-Rate Factors,” Tech. Rep. ANSI/ANS 6.1.1-1977, American Nuclear Society, La Grange Park, IL, USA, 1977.
- [13] Dassault Systèmes Simulia Corp., “Abaqus/CAE 6.12 Online Documentation,” 2012.
- [14] R. L. Martz, “The MCNP6 Book on Unstructured Mesh Geometry: User’s Guide,” Tech. Rep. LA-UR-11-05668 Rev 8, Los Alamos National Laboratory, Los Alamos, NM, USA, 2014.
- [15] J. A. Kulesza and R. L. Martz, “MCNP6 Unstructured Mesh Tutorial Using Abaqus/CAE 6.12-1,” Tech. Rep. LA-UR-15-25143, Los Alamos National Laboratory, Los Alamos, NM, USA, 2015.
- [16] C. A. Brewer, “Color Brewer 2.” <http://www.colorbrewer2.org/>. Accessed: 2015-08-10.
- [17] R. D. Mosteller, S. C. Frankle, and P. G. Young, “Data Testing of ENDF/B-VI with MCNP: Critical Experiments, Thermal-Reactor Lattices, and Time-of-Flight Measurements,” Tech. Rep. LA-UR-96-2143, Los Alamos National Laboratory, Los Alamos, NM, USA, 1996.

Tables

- I Pulsed Sphere UM Parameter Summary (Min. Edge Length = 0.010 cm)
- II Fractional Errors For Pulsed Sphere Calculated Spectra

Table I: Pulsed Sphere UM Parameter Summary (Min. Edge Length = 0.010 cm)

Experiment	Refinement	Max. d/h	Nodes	Elements
Beryllium	Fine	0.005	15517	70151
	Medium	0.010	8759	36249
	Coarse	0.020	3260	15074
Carbon	Fine	0.005	10297	46190
	Medium	0.010	6583	27923
	Coarse	0.020	4469	18754
Concrete	Fine	0.005	16112	73409
	Medium	0.010	7846	33695
	Coarse	0.020	4684	19585
Iron	Very Fine	0.0025	9332	42742
	Fine	0.005	3117	12470
	Medium	0.010	720	2777
	Coarse	0.020	217	885
Water	Fine	0.005	48018	195071
	Medium	0.010	41552	167939
	Coarse	0.020	25790	99104
Lithium	Fine	0.005	110790	376903
	Medium	0.010	77460	274125
	Coarse	0.020	34411	123293

Table II: Fractional Errors For Pulsed Sphere Calculated Spectra

Experiment	Detailed	CSG		Fine	UM	
		Hybrid	Legacy		Medium	Coarse
Beryllium	0.136	0.137	0.054	0.054	0.054	0.054
Carbon	0.161	0.165	0.092	0.093	0.092	0.092
Concrete	0.146	0.156	0.244	0.243	0.243	0.241
Iron*	0.079	0.093	0.210	0.248	0.248	0.249
Water	0.234	0.234	0.175	0.192	0.191	0.191
Lithium	0.013	0.013	0.011	0.009	0.009	0.009

*Very Fine UM Fractional Error: 0.248

Figures

- 1 Pulsed Sphere Geometries Reformatted from Ref. 1 (Dimensions are Centimeters)
- 2 Ueki Benchmark Geometry (Dimensions are Centimeters)
- 3 Pulsed Sphere Time-of-Flight Spectra for CSG and UM Cases (All Results Include $\pm 1\sigma$ Uncertainty Bars)
- 4 Normalized Ueki Neutron Attenuation Curves for CSG and Purely UM Calculations Relative to Experimental Values
- 5 Normalized Ueki Neutron Attenuation Curves for Hybrid CSG/UM Calculations (Paraffin as UM, Shield/Detector as CSG) Relative to Experimental Values
- 6 Normalized Ueki Neutron Attenuation Curves for Hybrid CSG/UM Calculations (Paraffin as CSG, Shield/Detector as UM) Relative to Experimental Values
- 7 Ueki Perspective Half-Space Neutron Flux (F4) Element-Wise Edits

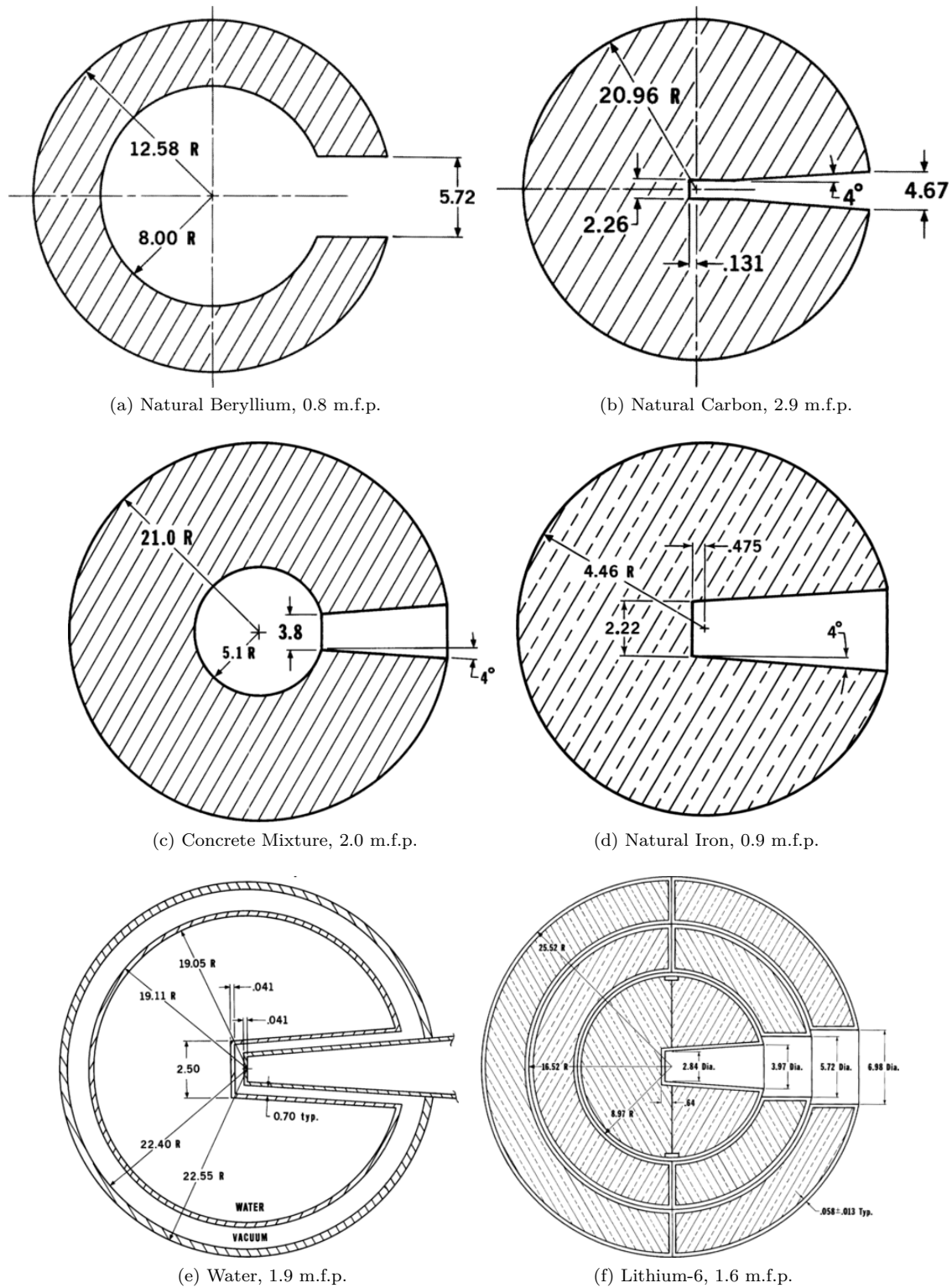


Figure 1: Pulsed Sphere Geometries Reformatted from Ref. 1 (Dimensions are Centimeters)

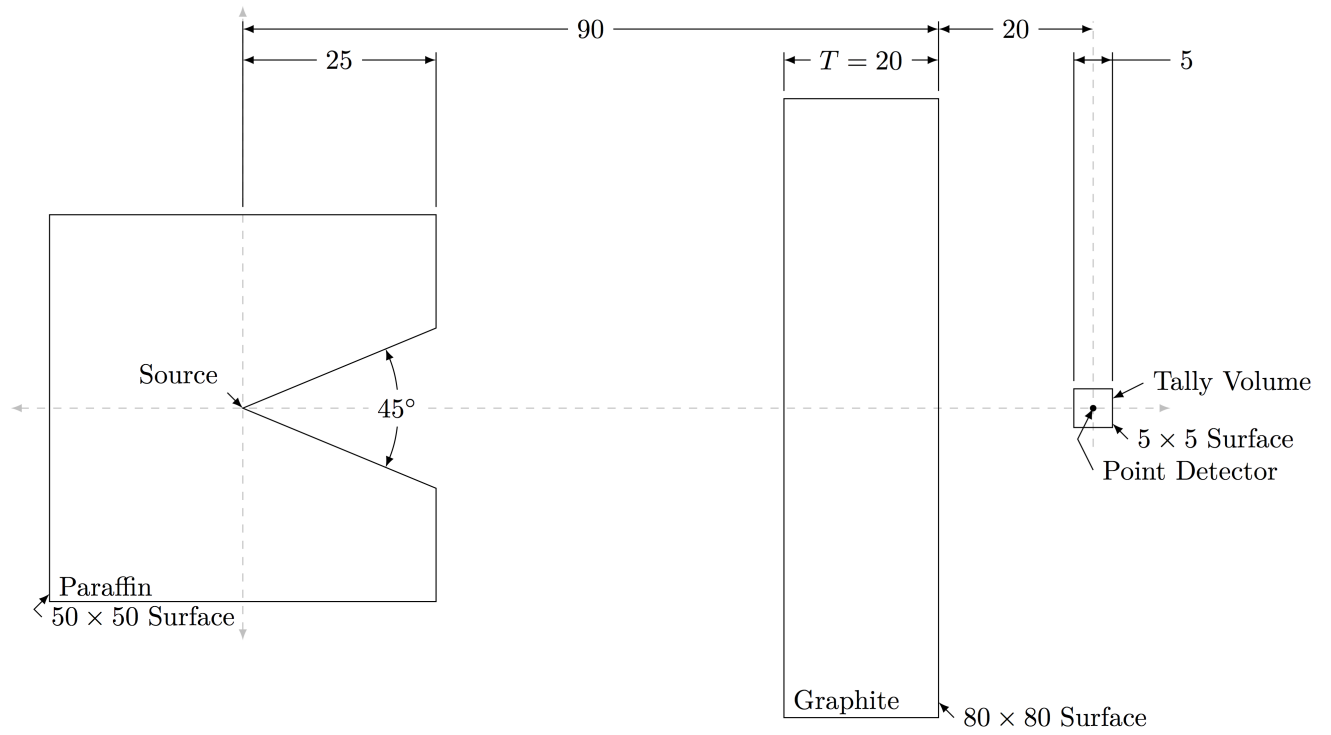


Figure 2: Ueki Benchmark Geometry (Dimensions are Centimeters)

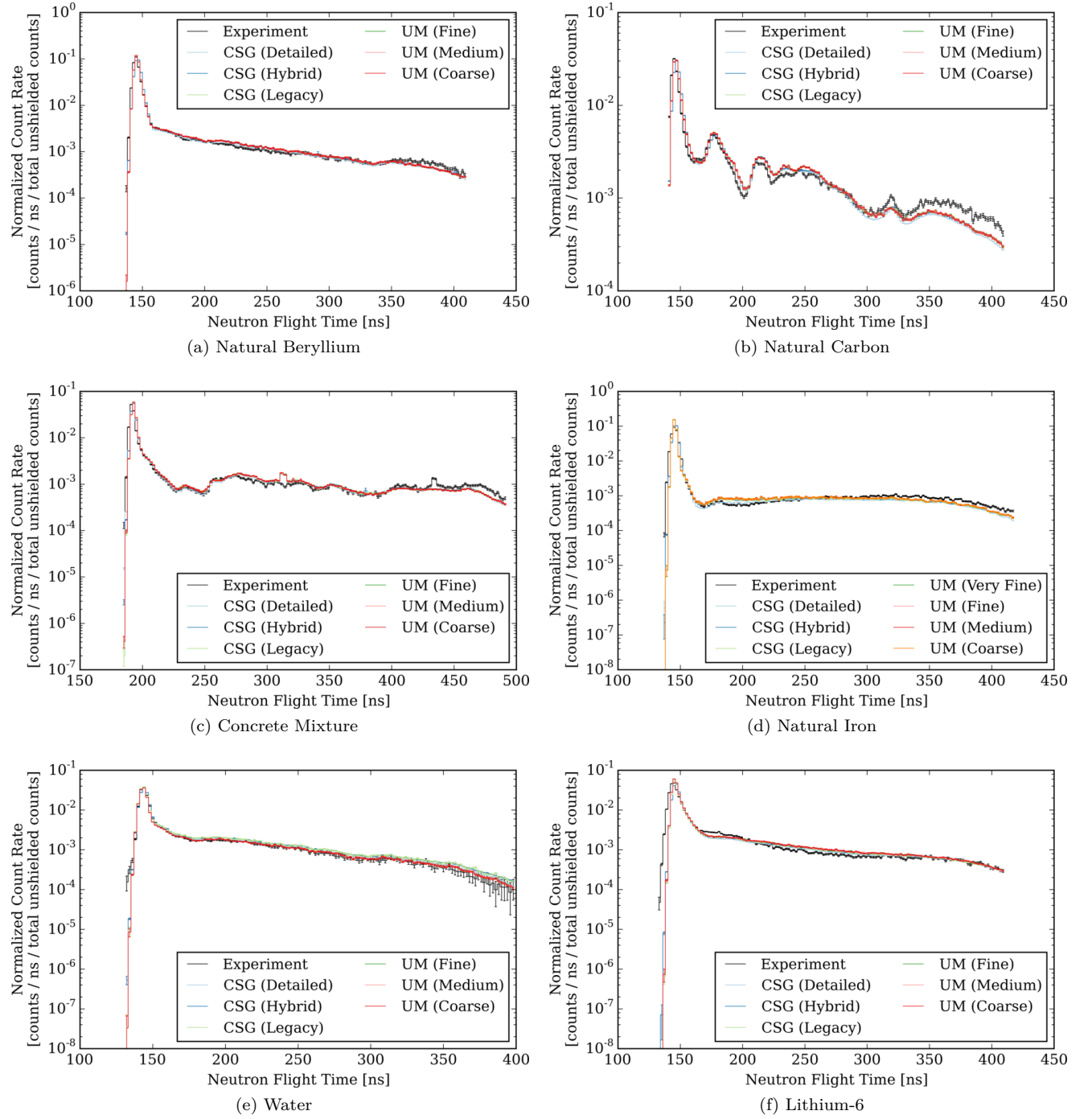


Figure 3: Pulsed Sphere Time-of-Flight Spectra for CSG and UM Cases (All Results Include $\pm 1\sigma$ Uncertainty Bars)

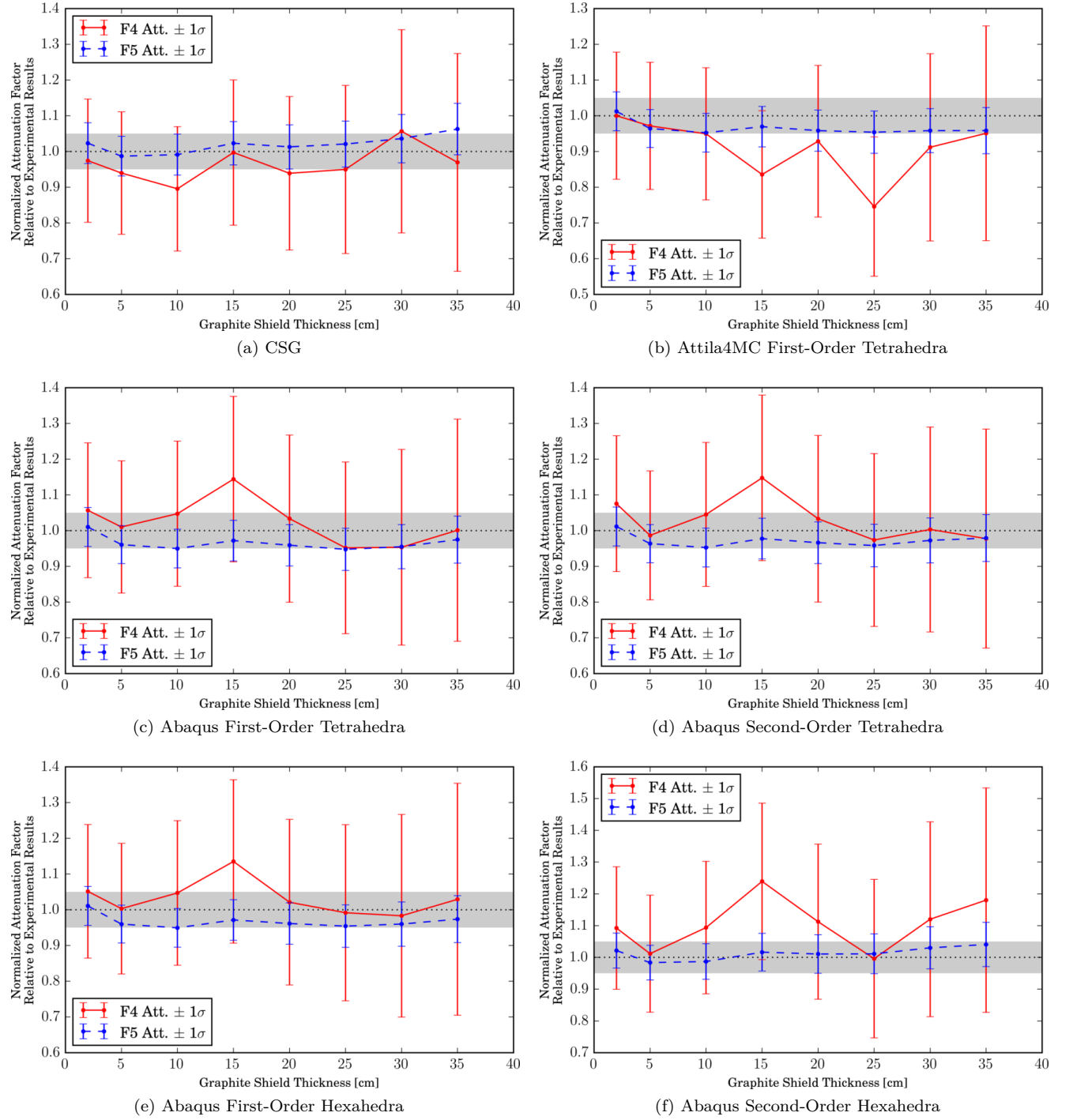
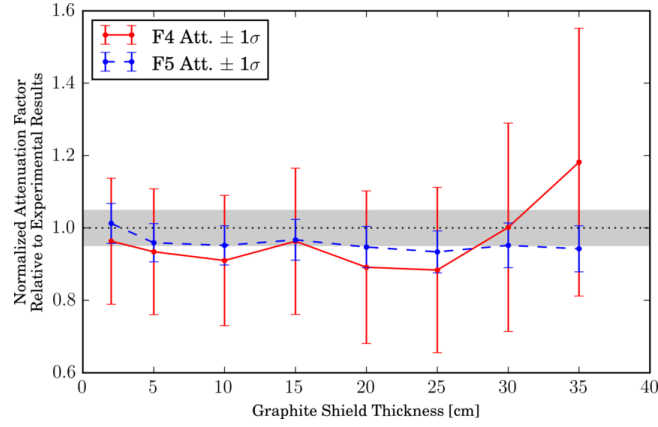
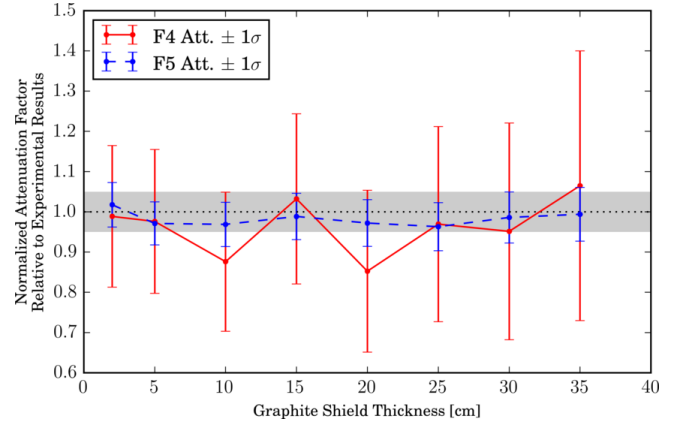


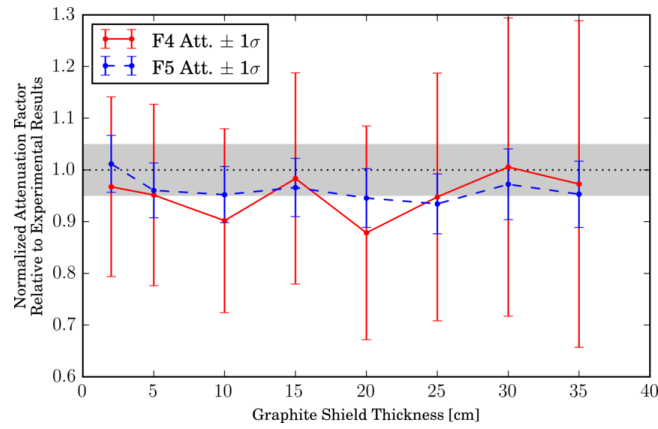
Figure 4: Normalized Ueki Neutron Attenuation Curves for CSG and Purely UM Calculations Relative to Experimental Values



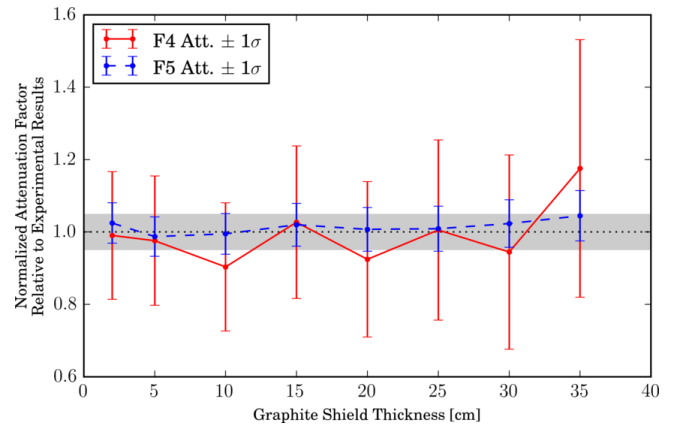
(a) Abaqus First-Order Tetrahedra



(b) Abaqus Second-Order Tetrahedra

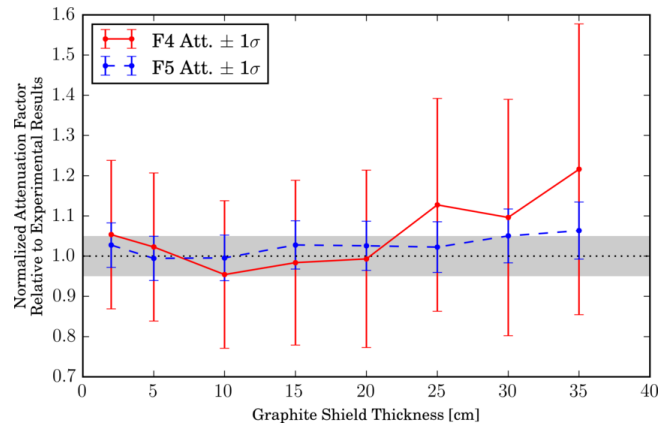


(c) Abaqus First-Order Hexahedra

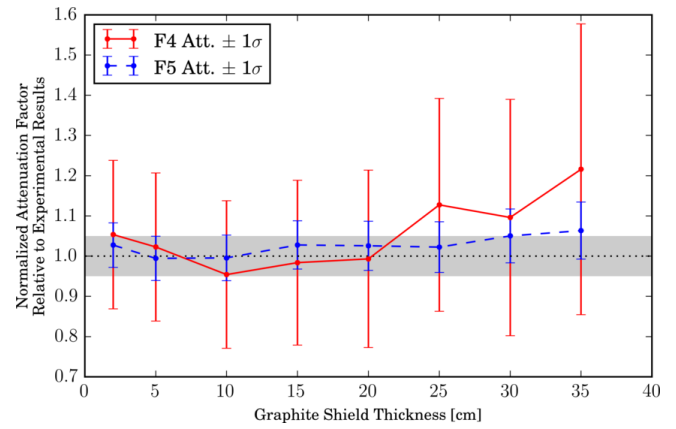


(d) Abaqus Second-Order Hexahedra

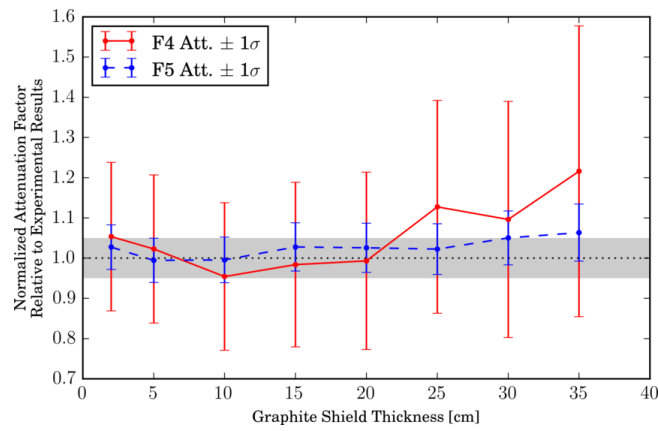
Figure 5: Normalized Ueki Neutron Attenuation Curves for Hybrid CSG/UM Calculations (Paraffin as UM, Shield/Detector as CSG) Relative to Experimental Values



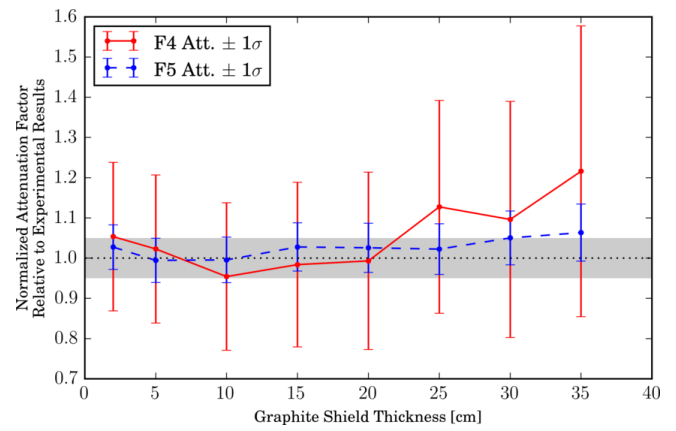
(a) Abaqus First-Order Tetrahedra



(b) Abaqus Second-Order Tetrahedra

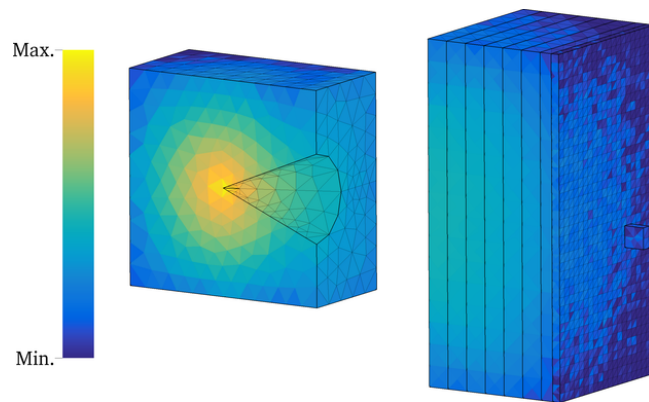


(c) Abaqus First-Order Hexahedra

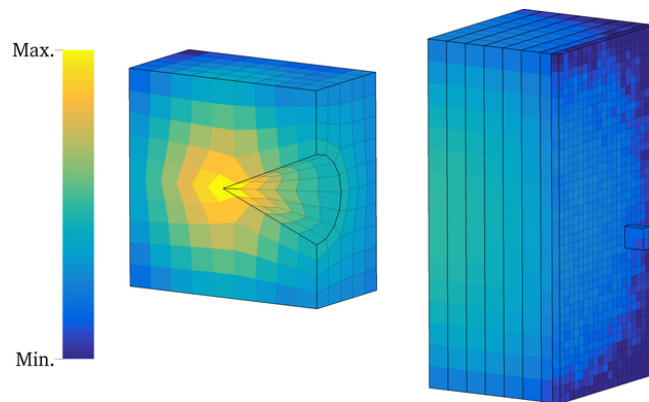


(d) Abaqus Second-Order Hexahedra

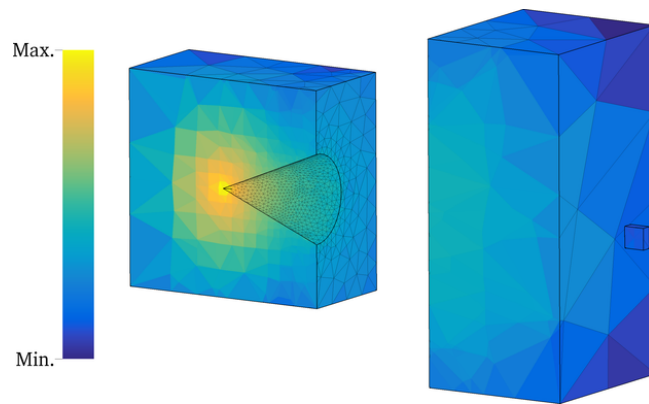
Figure 6: Normalized Ueki Neutron Attenuation Curves for Hybrid CSG/UM Calculations (Paraffin as CSG, Shield/Detector as UM) Relative to Experimental Values



(a) Abaqus First-Order Tetrahedra



(b) Abaqus First-Order Hexahedra



(c) Attila4MC First-Order Tetrahedra

Figure 7: Ueki Perspective Half-Space Neutron Flux (F4) Element-Wise Edits